RAA 2017 Vol. **17** No. **8**, 79 (8pp) doi: 10.1088/1674–4527/17/8/79

http://www.raa-journal.org *http://iopscience.iop.org/raa*

Research in Astronomy and Astrophysics

Red Clump Stars from LAMOST II: the outer disc of the Milky Way

Jun-Chen Wan[1,2], Chao Liu[1] and Li-Cai Deng[1]

[1] Key Laboratory of Optical Astronomy, National Astronomical Observatories, Chinese Academy of Sciences, Beijing 100012, China; *junchenwan@bao.ac.cn*

[2] University of Chinese Academy of Sciences, Beijing 100049, China

Received 2017 March 13; accepted 2017 April 14

Abstract We present stellar density maps of the Galactic outer disc with red clump stars from LAMOST data. These samples are separated into younger (mean age $\sim$ 2.7 Gyr) and older (mean age $\sim$ 4.6 Gyr) populations so that they can trace the variation of structures with ages in the range of Galactocentric radius R from 9 to 13.5 kpc. We show that scale heights for both of the two populations increase with R and display radial gradients of 48 ± 6 and 40 ± 4 pc kpc^{-1} for the older and younger populations, respectively. It is evident that flaring occurs in the thin disc populations with a wide range of ages. Moreover, the intensity of flaring does not seem to be significantly related to the age of the thin disc populations. On the other hand, scale lengths of the radial surface density profiles are 4.7 ± 0.5 kpc for the younger population and 3.4 ± 0.2 kpc for the older population, meaning that the younger disc population is more radially extended than the older one. Although the fraction of the younger population mildly increases from 28% at $R \sim 9$ to about 35% at $R \sim 13$ kpc, the older population is prominent with a fraction of no less than 65% in the outer disc.

Key words: Galaxy: disc — Galaxy: evolution — Galaxy: structure

1 INTRODUCTION

Although they are often very faint and do not contain many stars, the outskirts of galaxies reflect the nature of the formation and evolution of galactic discs. Simulations show that secular evolution of the discs can significantly alter their properties, from the age distribution to the stellar density profile of the outer disc (Roškar et al. 2008; Debattista et al. 2006). In addition, the discs are more easily perturbed either by dynamical torques or by new infalling gas. As a consequence, a warp can be induced in their outskirts (Shen & Sellwood 2006; Roškar et al. 2010). Minor mergers may also affect the outer discs and induce substructures in stellar density as well as in kinematics (Gómez et al. 2013, 2016).

However, observations of the outskirts of disc galaxies are not trivial. In principle, the surface brightness of outer discs is extremely faint and imaging of the outskirt regions often suffers from a very low signal-to-noise ratio. Nevertheless, Pohlen & Trujillo (2006) classified several hundred external galaxies by their surface luminosity distributions and found that the outer discs show three different types of profiles: exponential, down-bending and up-bending. Zheng et al. (2015) also showed that the surface brightness profiles of disc galaxies are broken in bluer bands, but they show unbroken exponential profiles in redder bands. The mechanisms leading to these differences are not quite clear so far.

For the case of the Milky Way, observations of individual stars are greatly advantageous in studies of the Galactic outer disc. López-Corredoira et al. (2002) fitted exponential density distribution models of the disc by using 2MASS red clump (RC) stars and found that the Galactic outer disc is substantially flared and warped. They suggested that the flaring disc can be described with an exponentially increasing scale height with radius. Moreover, a puzzling substructure, the Monoceros ring, in the Galactic Anti-center direction has been unveiled by Newberg et al. (2002) from the star count of turnoff stars. Momany et al. (2006) claimed that this is likely to be the effect of the warp and flare by using RC stars and giant stars selected from 2MASS. Gómez et al. (2016) analyzed the vertical structure in simulations, and their results showed that interactions among the satellites, Galactic halo and disc can also induce such kind of feature. Furthermore, Xu et al. (2015) discovered that

star counts in the north and south of the Galactic mid-plane of the outer disc are not symmetric but rather display wave-like oscillations. Recently, Liu et al. (2017b) found that the disc has no truncation but exponentially expands to 19 kpc and then smoothly transitions to the stellar halo.

Not only are the spatial structures quite complicated, but stellar kinematics in the outer disc also deviate from axisymmetry. Tian et al. (2016) showed that the mean radial velocity is not zero but rather varies from -6 to $+7\,\mathrm{km\ s^{-1}}$ with Galactocentric radius from 7 to 14 kpc with RC stars from LAMOST data. Such an oscillating radial velocity may be associated with perturbation induced by the rotating bar or spiral arms. Meanwhile, Liu et al. (2017a) demonstrated that the stellar warp may also lead to vertical peculiar velocity in some directions, especially for young stars.

The nature of the outer disc can be examined not only from spatial structures and stellar kinematics, but also from the features of stellar populations. In general, chemical abundances and age can characterize stellar populations well. However, elemental abundances can only be available from high signal-to-noise and high spectral resolution data, which are rarely observed in the outer disc. On the other hand, the age of field stars is probably the hardest quantity to be determined. To avoid non-trivial works of determining the age for individual stars, we turn to use some special tracers for stellar disc populations with different ages.

In this work, we select RC stars obtained from the LAMOST survey (Cui et al. 2012; Zhao et al. 2012) as tracers and compare the structural parameters between younger and older RC populations. The LAMOST survey has covered the Galactic Anti-center region well due to special conditions associated with the site of the telescope (Deng et al. 2012; Yao et al. 2012). Thus, it can sample the Galactic outer disc beyond the location of the Sun well.

The paper is organized as follows. In Section 2, we outline the RC star catalog identified from LAMOST data, purifying and separating the RC candidate samples and the methods to derive stellar density profiles with spectroscopic data. In Section 3, we show the stellar density maps for younger and older RC populations. The scale heights as functions of R and scale lengths for the two populations are determined. The fraction of the younger population varying with R is also demonstrated in this section. In Section 4, we discuss the influence from interstellar extinction and warp, and compare our results with others. In the same section, we briefly draw conclusions.

2 DATA

Wan et al. (2015) (hereafter, Paper I) identified more than 100 000 RC candidates with [Fe/H]> -0.6 dex from the LAMOST DR2 catalog using seismic calibrated surface gravities from Liu et al. (2015). The LAMOST DR2 published [Fe/H] and Teff parameters were determined by the LASP pipeline (LAMOST Stellar Parameter Pipeline, Wu et al. 2011, 2014). We adopt a similar approach to identify more RC candidates from the LAMOST DR3 catalog, which totally contains more than 4 million stellar spectra.

Then, we apply the criteria suggested by Tian et al. (2016) (hereafter, Paper II) to purify the RC candidate samples. Paper II drew the distribution of RC candidates in the [Fe/H] vs. $\mathrm{Mg_b}$ plane, and adopted an empirical separation line to remove red giant branch (RGB) stars (see their fig. 1). Although $\mathrm{Mg_b}$ is an α element, it is more sensitive to $\log g$ and $T_{\rm eff}$. Therefore, [Fe/H] vs. $\mathrm{Mg_b}$ should not significantly reflect the α-abundance. It is also noted that, according to Hayden et al. (2015), the outer disc is dominated by low-α stars. In other words, the RC stars should not cover a large range of α abundances. Generally speaking, with the same [Fe/H] and $\log g$, RC stars have larger $T_{\rm eff}$ than RGB stars. On the other hand, with the same [Fe/H] and $\log g$, RC stars have smaller $\log g$. Therefore, RC stars and RGB stars should be separated in the [Fe/H] vs. $\mathrm{Mg_b}$ relation. In order to verify the separation line, Paper II overlaid the cross-matched RC stars from Stello et al. (2013), who used seismic period and frequency to accurately classify primary and secondary RC stars, and RGB stars. Paper II found that about 97% of seismically-identified RC stars are classified by the empirical separation line and the value is 94% for RGB stars.

Paper II also suggested separating the RC samples into younger and older populations from the effective temperature–surface gravity–metallicity space. Because the initial stellar masses of secondary RC stars ($\sim 2\,M_{\odot}$) are larger than primary ones, secondary RC stars have non-degenerate helium-burning cores. The different evolution tracks for primary and secondary RC stars can be present at different positions in the $T_{\rm eff}$-$\log g$ plane. Paper II used PARSEC isochrones (Bressan et al. 2012) to distinguish RC stars younger or older than 2 Gyr in the $T_{\rm eff}$-$\log g$ plane with different metallicities (see their fig. 2). According to Paper II (see their fig. 3), the younger RC population (hereafter RCyoung), which has a mean age of about 2.7 Gyr (covering age from $\sim$1 Gyr to 6 Gyr), is dominated by secondary RC stars, while the older RC population (hereafter RCold) is dominated by primary RC stars with a mean age of about 4.6 Gyr (cov-

ering age from 1 Gyr to 10 Gyr). Both RC populations are younger than typical thick disc or halo populations, but the difference in age is sufficiently large to distinguish the temporal effect in the structure of the thin disc.

We finally select 73 278 RCold stars and 32 423 RCyoung stars. Their distances are estimated according to Paper I, where the absolute magnitudes of RC stars are fitted with isochrones and exhibit a distance uncertainty of about 10%. The spatial coordinates for these samples are converted to Galactocentric cylindrical coordinates in which R and Z represent the Galactocentric radius and height above the Galactic mid-plane, respectively. We adopt the Sun position: $R_0 = 8$ and $Z_0 = 0.027$ kpc (Chen et al. 2001). The RC stars are mostly located from 150° to 210° in Galactic longitude and cover the outer disc from $R \sim 9$ to 14 kpc well.

Moreover, Liu et al. (2017b) developed a statistical method to derive the stellar density for a certain stellar population. According to this approach, stellar densities have been determined separately for all the RC samples (i.e., RCold+RCyoung, hereafter RCall), and for the RCold and RCyoung samples.

3 RESULTS

Figure 1 presents stellar density maps in the R–Z plane for the RCall, RCold and RCyoung populations from top to bottom, respectively. First, it clearly shows from the color coded $\ln \nu$ that the disc of the RCyoung population is substantially thinner than that of the RCold population. Second, the color coded logarithmic stellar densities indicate that the RCyoung population is less dense than the RCold population. This means that the stellar outer disc is dominated by older populations. The density map for RCall is more similar to that for RCold, confirming that the older population is indeed prominent.

To quantify the structures accounting for complicated radial features in the outskirts, e.g. the flare, we split the stars into various R bins and fit the 1-D vertical density profile along Z in each R bin. We assume that the disc is composed of two components and the density profile is separable about R and Z such that

$$\nu(R, Z) = \nu(R|Z = 0)\,(\nu_{\rm thin}(Z|R) + \nu_{\rm thick}(Z|R))\,, \quad (1)$$

where $\nu(R|Z = 0)$ is the stellar density at $Z = 0$. The two disc components in the right-hand side follow hyperbolic secant squared profiles (Kruit 1998)

$$\nu_{\rm thin}(Z|R) = (1 - f_t(R))\,{\rm sech}^2\left(\frac{Z}{2h_{z,{\rm thin}}(R)}\right) \quad (2)$$

and

$$\nu_{\rm thick}(Z|R) = f_t(R){\rm sech}^2\left(\frac{Z}{2h_{z,{\rm thick}}(R)}\right), \quad (3)$$

where $h_{z,{\rm thin}}(R)$ and $h_{z,{\rm thick}}(R)$ are the scale heights of the thin and thick components, respectively, and $f_t(R)$ is the fraction of the thick component. Because RC stars are mostly metal-rich and they are selected with [Fe/H]> -0.6 dex (Wan et al. 2015), only very few halo stars should be included in the samples. Therefore, the halo component in the star count model is negligible.

The data are separated into 10 R bins from 9 to 13.5 kpc with a bin size of 0.5 kpc. At each R bin, we fit the disc model described by Equations (1)–(3) with the Markov chain Monte Carlo technique[1] for RCall, RCold and RCyoung. The best-fit model parameters with uncertainties are listed in Table 1.

Note that the thick disc population may not be completely sampled since the cut of [Fe/H]> -0.6 dex removes lots of metal-poor thick disc stars. Therefore, in this work, we only focus on the thin disc components.

The best-fit scale heights of the thin disc component for RCall, RCyoung and RCold are shown in Figure 2 with black, blue and red dots, respectively. Over all R bins, the scale heights for RCyoung are smaller than those for the RCold population by a factor of 82%. In other words, RCyoung is consistently thinner than RCold in the range of R from 9 to 13.5 kpc. This is expected if the thin disc is heated by giant molecular clouds. In such a scenario, the older population has been heated for a longer time and hence is thicker than the younger one.

It is also clearly evident that the flare is found in both RCyoung and RCold populations. Indeed, the scale heights increase from ~ 150 pc at $R = 9$ kpc to about 400 pc at $R = 13.5$ kpc for both populations. Although the increasing h_z shows some oscillations, the flare can be empirically fitted with a linear model within the detected range of R. The dashed lines shown in the figure represent the best linear fits of h_z as a function of R for populations with the same colors. The radial gradients of the scale heights are 45 ± 5, 48 ± 6 and 40 ± 4 pc kpc^{-1} for the RCall, RCold and RCyoung populations, respectively. The gradients for the RCyoung and RCold populations are not significantly different, implying that the intensity of the flaring does not seem to be closely related to the age of the thin disc populations.

We then compare the flare from our result with López-Corredoira et al. (2002), who modeled the flaring of the disc with an exponential function of R. Note that López-Corredoira et al. (2002) adopted an exponentially declining vertical profile, while we apply a ${\rm sech}^2$ form. The scale height of the exponential profile is larger than that of the ${\rm sech}^2$ profile by about a factor of 2. Therefore,

[1] We use the *emcee* package (Foreman-Mackey et al. 2013) to run the Markov chain Monte Carlo simulation.

Table 1 The Best-Fit Model Parameters and Their Uncertainties for the Vertical Density Profiles at Various R Bins

R (kpc)		9.0	9.5	10.0	10.5	11.0
$\mathrm{RC_{all}}$	$\ln\nu(R)$	$-7.02^{+0.02}_{-0.01}$	$-7.53^{+0.02}_{-0.02}$	$-7.87^{+0.02}_{-0.01}$	$-8.12^{+0.02}_{-0.02}$	$-8.31^{+0.02}_{-0.02}$
	$h_{z,\mathrm{thin}}$ (pc)	$166.3^{+2.3}_{-2.2}$	$211.7^{+3.4}_{-3.4}$	$245.5^{+5.1}_{-5.1}$	$270.8^{+7.1}_{-6.3}$	$292.2^{+9.8}_{-9.5}$
	$h_{z,\mathrm{thick}}$ (pc)	$641.7^{+1.4}_{-1.2}$	$647.1^{+3.3}_{-2.1}$	$651.9^{+2.7}_{-4.2}$	$648.2^{+5.3}_{-5.4}$	$650.1^{+7.3}_{-8.2}$
	f_t	$0.032^{+0.002}_{-0.003}$	$0.054^{+0.005}_{-0.005}$	$0.083^{+0.008}_{-0.009}$	$0.123^{+0.014}_{-0.013}$	$0.137^{+0.019}_{-0.019}$
$\mathrm{RC_{old}}$	$\ln\nu(R)$	$-7.42^{+0.02}_{-0.01}$	$-7.92^{+0.01}_{-0.02}$	$-8.26^{+0.02}_{-0.02}$	$-8.55^{+0.02}_{-0.02}$	$-8.74^{+0.02}_{-0.02}$
	$h_{z,\mathrm{thin}}$ (pc)	$176.3^{+2.6}_{-2.5}$	$226.3^{+3.9}_{-3.8}$	$259.1^{+6.1}_{-6.2}$	$294.4^{+9.1}_{-8.8}$	$326.2^{+13.0}_{-13.5}$
	$h_{z,\mathrm{thick}}$ (pc)	$648.1^{+3.4}_{-2.1}$	$650.2^{+3.3}_{-2.9}$	$653.4^{+4.1}_{-7.2}$	$641.5^{+11.3}_{-6.4}$	$651.8^{+12.2}_{-17.3}$
	f_t	$0.038^{+0.003}_{-0.003}$	$0.063^{+0.006}_{-0.006}$	$0.099^{+0.012}_{-0.011}$	$0.139^{+0.012}_{-0.019}$	$0.143^{+0.028}_{-0.030}$
$\mathrm{RC_{young}}$	$\ln\nu(R)$	$-8.11^{+0.02}_{-0.01}$	$-8.64^{+0.02}_{-0.02}$	$-8.99^{+0.02}_{-0.02}$	$-9.18^{+0.02}_{-0.02}$	$-9.34^{+0.02}_{-0.02}$
	$h_{z,\mathrm{thin}}$ (pc)	$146.2^{+1.6}_{-1.5}$	$183.9^{+2.2}_{-2.2}$	$222.1^{+3.6}_{-3.4}$	$236.3^{+4.7}_{-4.4}$	$255.7^{+6.2}_{-5.9}$
	$h_{z,\mathrm{thick}}$ (pc)	$655.7^{+2.4}_{-4.3}$	$652.1^{+2.8}_{-3.1}$	$649.7^{+5.0}_{-4.3}$	$653.6^{+4.9}_{-6.4}$	$650.9^{+9.3}_{-8.7}$
	f_t	$0.015^{+0.001}_{-0.001}$	$0.033^{+0.002}_{-0.003}$	$0.045^{+0.004}_{-0.005}$	$0.076^{+0.007}_{-0.007}$	$0.081^{+0.009}_{-0.009}$
R (kpc)		11.5	12.0	12.5	13.0	13.5
$\mathrm{RC_{all}}$	$\ln\nu(R)$	$-8.47^{+0.02}_{-0.02}$	$-8.64^{+0.02}_{-0.03}$	$-8.69^{+0.06}_{-0.05}$	$-8.89^{+0.07}_{-0.06}$	$-9.16^{+0.07}_{-0.06}$
	$h_{z,\mathrm{thin}}$ (pc)	$303.1^{+12.3}_{-11.8}$	$328.1^{+15.9}_{-15.3}$	$315.7^{+25.2}_{-23.2}$	$334.1^{+31.2}_{-28.1}$	$424.2^{+28.7}_{-40.3}$
	$h_{z,\mathrm{thick}}$ (pc)	$648.6^{+13.4}_{-9.2}$	$657.1^{+10.1}_{-12.5}$	$654.9^{+16.7}_{-20.0}$	$649.9^{+25.3}_{-15.4}$	$655.2^{+27.1}_{-28.2}$
	f_t	$0.175^{+0.021}_{-0.022}$	$0.190^{+0.026}_{-0.030}$	$0.193^{+0.030}_{-0.035}$	$0.221^{+0.038}_{-0.045}$	$0.132^{+0.098}_{-0.088}$
$\mathrm{RC_{old}}$	$\ln\nu(R)$	$-8.93^{+0.02}_{-0.03}$	$-9.12^{+0.03}_{-0.03}$	$-9.21^{+0.05}_{-0.06}$	$-9.36^{+0.07}_{-0.06}$	$-9.62^{+0.06}_{-0.06}$
	$h_{z,\mathrm{thin}}$ (pc)	$325.7^{+16.5}_{-15.8}$	$366.3^{+23.8}_{-21.9}$	$354.8^{+34.7}_{-31.2}$	$346.5^{+36.6}_{-32.6}$	$445.6^{+23.5}_{-32.1}$
	$h_{z,\mathrm{thick}}$ (pc)	$649.0^{+22.4}_{-21.2}$	$654.1^{+20.7}_{-22.1}$	$652.2^{+26.4}_{-28.2}$	$658.2^{+28.9}_{-25.4}$	$649.0^{+47.1}_{-28.0}$
	f_t	$0.218^{+0.032}_{-0.035}$	$0.217^{+0.046}_{-0.056}$	$0.211^{+0.049}_{-0.069}$	$0.260^{+0.045}_{-0.057}$	$0.101^{+0.113}_{-0.070}$
$\mathrm{RC_{young}}$	$\ln\nu(R)$	$-9.46^{+0.02}_{-0.02}$	$-9.59^{+0.02}_{-0.03}$	$-9.65^{+0.06}_{-0.05}$	$-9.83^{+0.08}_{-0.07}$	$-10.12^{+0.08}_{-0.07}$
	$h_{z,\mathrm{thin}}$ (pc)	$262.4^{+7.3}_{-7.2}$	$286.1^{+9.3}_{-8.9}$	$301.3^{+17.2}_{-16.1}$	$289.2^{+23.1}_{-19.2}$	$370.0^{+38.9}_{-38.4}$
	$h_{z,\mathrm{thick}}$ (pc)	$644.7^{+8.4}_{-7.2}$	$657.0^{+10.9}_{-9.3}$	$650.8^{+22.2}_{-17.2}$	$652.9^{+21.3}_{-20.8}$	$654.1^{+38.9}_{-39.1}$
	f_t	$0.100^{+0.011}_{-0.011}$	$0.109^{+0.013}_{-0.013}$	$0.107^{+0.019}_{-0.022}$	$0.210^{+0.024}_{-0.025}$	$0.174^{+0.060}_{-0.081}$

we divide the scale height model of López-Corredoira et al. (2002) by 2 so that they can be compared with our result. The black solid line in the figure indicates the rescaled flaring scale height from López-Corredoira et al. (2002). It is quite similar to the scale heights from this work at $R < 11$ kpc. However, at $R > 11$ kpc, the flaring scale heights modeled by López-Corredoira et al. (2002) are significantly larger than our result. The discrepancy at $R > 11$ kpc may be caused by the different areas of the sky covered by each sample, or the different methods used to select RC stars. López-Corredoira et al. (2002) selected RC stars from infrared photometry, while we select them from spectroscopic data.

López-Corredoira & Molgó (2014) modeled the flare with a quadratic function of R, which is shown as the green dotted line and three green squares with error bars to indicate the uncertainties in Figure 2. (It is also divided by 2 to align with our sech^2 scale height.) Although the gradient of the scale height from López-Corredoira & Molgó (2014) is quite similar to ours, the values of scale height are smaller than ours. Note that López-Corredoira & Molgó (2014) used F/G type dwarfs as tracers, which are younger than our samples. Normally, a younger population has a smaller scale height. Also, considering the larger uncertainties, their scale heights are only about 1-σ lower than our result, which is not statistically significant.

On the other hand, the surface stellar density, $\Sigma(R)$, can be derived by integrating the vertical profile over Z. For the sech^2 profile, it is easy to obtain that

$$\Sigma(R) = 4\Big((1-f_t(R))h_{z,\mathrm{thin}}(R) + f_t(R)h_{z,\mathrm{thick}}(R)\Big)\nu(R|Z=0). \quad (4)$$

The top panel of Figure 3 shows the stellar surface densities as functions of R for the populations of RCall (black dots), RCold (red dots) and RCyoung (blue dots). The dashed lines indicate the best fit exponential profiles of Σ for corresponding populations with the same color. The derived scale lengths are 3.7 ± 0.3, 3.4 ± 0.2 and 4.7 ± 0.5 kpc for RCall, RCold, and RCyoung, respectively. Note that the RCold population has larger scale height with smaller scale length, while the RCyoung population has smaller scale height with larger scale length. The trend that younger populations have larger scale

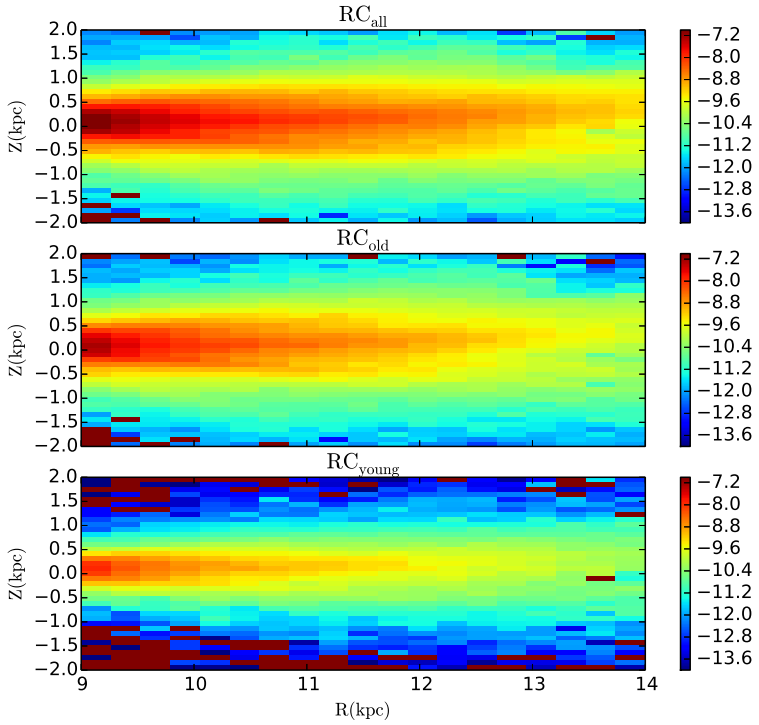

Fig. 1 The stellar density maps for RCall (*top panel*), RCold (*middle panel*) and RCyoung (*bottom panel*) in the R–Z plane. Colors indicate values of $\ln \nu$.

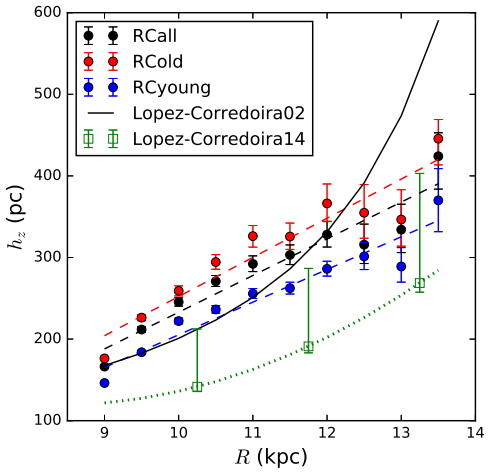

Fig. 2 The derived scale heights as functions of R for the RCall (*black dots*), RCold (*red dots*) and RCyoung (*blue dots*) populations. The dashed lines represent the best linear fits of scale heights for the corresponding populations with the same colors. The black solid line is the scale height from López-Corredoira et al. (2002) divided by 2. The green dotted line and three green squares with error bars indicate the scale height from López-Corredoira & Molgó (2014) divided by 2 as well.

length and smaller scale height is qualitatively consistent with Bovy et al. (2012).

The bottom panel of Figure 3 shows the ratio of the surface densities of the RCyoung to RCall populations, $\Sigma_y/\Sigma_{\rm all}$. It is around 28% at $R < 10$ kpc, while, at $R \sim 13$ kpc, $\Sigma_y/\Sigma_{\rm all}$ moderately increases to 35% with relatively larger uncertainty. This means that the relative number of younger stars becomes slightly larger in the outer disc, although the older population is still dominant in the outskirt region.

Note that Martig et al. (2016) claimed the median age of the RC stars located at $0 < |Z| < 0.5$ kpc

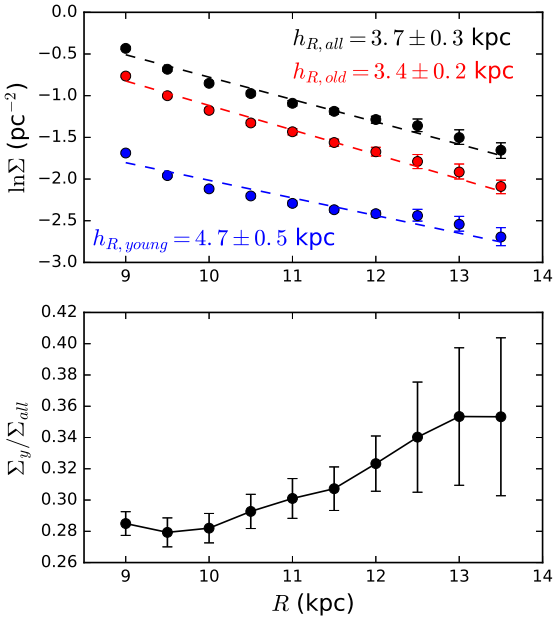

Fig. 3 The top panel displays surface stellar densities, in logarithmic form, as functions of R for the RCall (*black dots*), RCold (*red dots*) and RCyoung (*blue dots*) populations. The dashed lines represent the best fit exponential profiles for corresponding populations with the same colors. The bottom panel displays the ratio of surface density for the RCyoung to RCall populations.

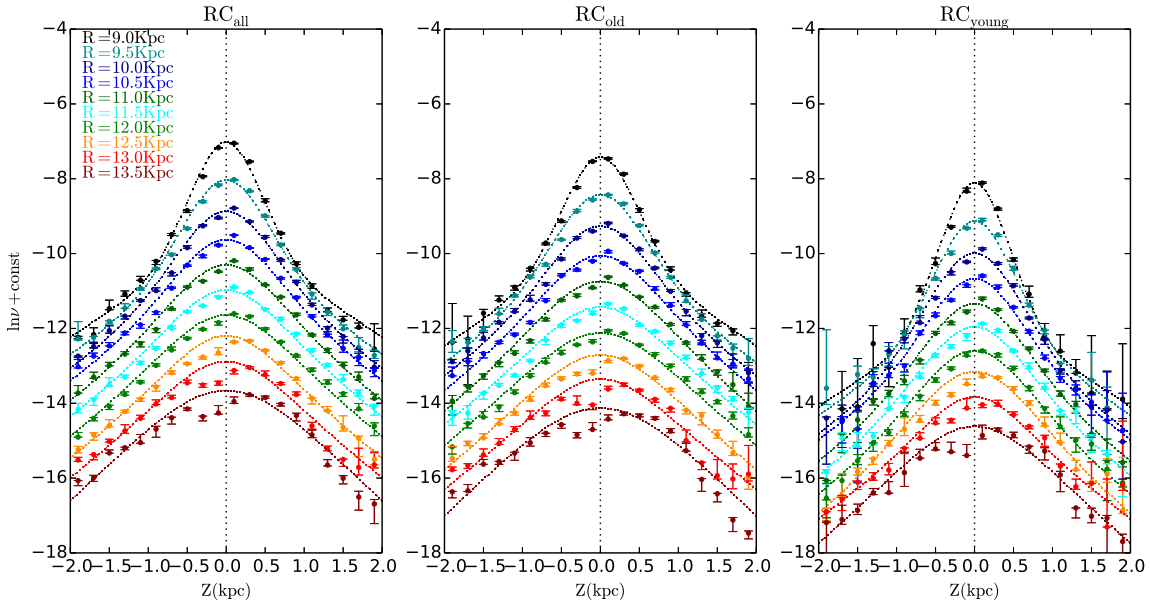

Fig. 4 The vertical density profiles for the RCall, RCold and RCyoung populations (from left panel to right panel respectively) in different R bins. The colors code the Galactocentric radii. The dashed lines stand for models described by Equations (1)–(3) corresponding to data with the same colors. In order to avoid overlapping, the vertical stellar density profiles are tiled with different offsets in $\ln\nu$ for different R bins.

decreases from about 8 Gyr at $R \sim 5$ kpc to 4 Gyr at ~ 8 kpc. From $R = 8$ to ~ 14 kpc, the median age is roughly flat or moderately declines (see their figures 1 and 3). By separating the stars into two populations with different ages, we show that the age distribution of the stellar populations may be variable at $9 < R < 13.5$ kpc in the sense that the fraction of younger stars slightly increases. However, this may not substantially alter the

median age of the whole outer disc, since the older population occupies more than 65% in this regime.

4 DISCUSSION AND CONCLUSIONS

In general, star counts along the Galactic disc often suffer from interstellar extinction. Although extinction is not severe in the Galactic Anti-center direction, it may still affect stellar density determinations.

Figure 1 shows an elongated shallow dip located between $R = 11$ and 14 kpc at $Z \sim -0.3$ kpc. It is very likely due to incompleteness of the photometric data induced by extinction. Indeed, Green et al. (2015) indicated that there are clouds with larger interstellar extinction located at a distance of 794–1995 pc, in the region $l \sim 180°$ and below $b = 0°$, which may be associated with the shallow dip.

Although interstellar extinction may affect stellar density measurements in some regions of the R–Z plane, especially in the south disc (the south disc represents $Z > 0$ and the north disc represents $Z < 0$), at Z close to 0, it does not play an important role in the overall shape of the vertical density profiles. Figure 4 shows that the vertical profiles for most of the R bins are fitted well by the models, except the lowest two profiles, which correspond to the two largest R bins. Even excluding the last two R bins, Figure 2 shows that the linearly increasing profiles are still substantial. Therefore, extinction does not change our result.

With data on the HI region in the outer Galactic disc, Levine et al. (2006) found asymmetry in the warp (especially at Galactocentric azimuth $90°$ and $-90°$, see figs. 6, 7 and 8 in their paper), which is claimed to be a prominent feature. However, in the Anti-center direction (the Galactocentric azimuth of which is around $0°$), the height of gas is almost 0 kpc at different Galactocentric radii (see figs. 6, 7 and 8 in their paper). López-Corredoira et al. (2002) also claimed that warped and unwrapped models provide equivalent fits to the data towards the Anti-center direction (at longitudes $150°$ to $210°$, see their fig. 14). Moreover, the LAMOST survey covers a larger area in the north disc than the south one at longitudes $180°$ to $210°$. On the other hand, at longitudes $150°$ to $180°$, the LAMOST survey covers a larger area in the south disc than the north one. Hence, the footprint of the LAMOST survey did not follow the warp of the Galactic disc, which means that the stellar vertical density distribution derived from LAMOST data should not be impacted by the Galactic warp. In other words, it is hard to confirm the geometry of the warp from LAMOST data in the Anti-center direction. Therefore, the dip shown at $11 < R < 14$ kpc is not likely due to asymmetry of the warp.

From the stellar density profiles, we find that the younger and older RC populations in the outer disc are significantly flared. The flaring disc traced by both populations shows increasing scale heights with Galactocentric radius R. The intensity of flaring does not seem to be substantially correlated with age of the thin disc populations. However, our RCyoung and RCold populations have age overlaps from 2 Gyr to 4 Gyr (see Sect. 2 and fig. 3 in Tian et al. (2016)). These age overlaps may cause the intensity of flaring for our two populations to likely be the same. On the other hand, the ages of most of our RC stars are younger than 6 Gyr, which may not be old enough to distinguish the difference in flaring from different populations.

The scale length of the surface density for the RCyoung population is 4.7 ± 0.5 kpc, which is significantly larger than the scale length of 3.4 ± 0.2 kpc for the RCold population. In addition, the scale heights for the RCyoung population are systematically smaller than those for the RCold population. Moreover, the fraction of the younger population is determined from the surface stellar density of the younger and older populations, which shows that the fraction of the RCyoung population moderately but consistently increases from 28% at $R = 9$ kpc to 35% at $R \sim 13$ kpc.

Liu et al. (2017b) claimed that the scale length of the thin disk is $\sim 1.6 \pm 0.1$ by using RGB stars from LAMOST data. This is quite smaller than our results, and is possibly because, in the mean, RGB stars are older than RC stars. More specifically, younger RGB stars are more massive than old RGB stars. A star with 2 $M_{\odot}$ at solar metallicity can only stay in the RGB stage for about 44 Myr, but can stay in the stage of helium-core burning for more than 100 Myr. For comparison, a star with a mass of 1 $M_{\odot}$ can stay in the stage of hydrogen-shell burning for more than 900 Myr and more than 100 Myr in the helium-core burning phase. Hence, young and massive stars have much less probability to be sampled in the RGB stage than in the RC stage (see table 5-2, Binney & Merrifield (1998)). Therefore, RGB stars and RC stars are two different populations, which exhibit different scale lengths. Moreover, RC stars used in this work have [Fe/H]> -0.6 dex, but in Liu et al. (2017b), RGB stars with a complete range of [Fe/H] are used to derive the surface stellar density profile. Although the age-metallicity relation is quite flat, metal-poor stars tend to be older than metal-rich ones. Therefore, averagely, the RGB stars are older than RC stars, which may have a smaller scale length.

Amores et al. (2017) identified a dependence of the thin disk scale length with age by using 2MASS data and they found that the value of scale length is in the range from $\sim$3.8 kpc (for the youngest stars (< 1 Gyr) in their sample) to $\sim$2.0 kpc (for the oldest stars (~ 8.5 Gyr) in their sample). Their value of scale length for the youngest stars is similar to our results, but for the oldest stars, their value is smaller than ours. The reason may be that their youngest samples have similar ages to ours and the oldest samples are older than ours.

It is reasonable to check our results with the RC sample cut at other ages. Unfortunately, our isochrone-based separation lines for RC populations (see Sect. 2) cannot be changed, because it is essentially determined by the helium-flash mass. If we change our separation lines, there would be more younger RC stars to contaminate the RCold population or more older RC stars to contaminate the RCyoung population (see fig. 2 in Tian et al. (2016)). In other words, our separation lines can only be at the age $\sim$ 2 Gyr. However, combined with other stellar tracers (such as dwarfs and turn-off stars), our samples could have a larger age range, which may be more appropriate for studying the dependence of disc structure with different populations. We will check this in the future.

Acknowledgements This work is supported by the National Key Basic Research Program of China 2014CB845700. CL acknowledges the National Natural Science Foundation of China under Grant Nos. 11373032 and 11333003. The Guo Shou Jing Telescope (the Large Sky Area Multi-Object Fiber Spectroscopic Telescope, LAMOST) is a National Major Scientific Project built by the Chinese Academy of Sciences. Funding for the project has been provided by the National Development and Reform Commission. LAMOST is operated and managed by National Astronomical Observatories, Chinese Academy of Sciences.

References

Amores, E. B., Robin, A. C., & Reyle, C. 2017, arXiv:1701.00475
Binney, J., & Merrifield, M. 1998, Galactic Astronomy (Princeton: Princeton Univ. Press)
Bovy, J., Rix, H.-W., Liu, C., et al. 2012, ApJ, 753, 148
Bressan, A., Marigo, P., Girardi, L., et al. 2012, MNRAS, 427, 127
Chen, B., Stoughton, C., Smith, J. A., et al. 2001, ApJ, 553, 184
Cui, X. Q., Zhao, Y. H., Chu, Y. Q., et al. 2012, RAA (Research in Astronomy and Astrophysics), 12, 1197
Debattista, V. P., Mayer, L., Carollo, C. M., et al. 2006, ApJ, 645, 209
Deng, L.-C., Newberg, H. J., Liu, C., et al. 2012, RAA (Research in Astronomy and Astrophysics), 12, 735
Foreman-Mackey, D., Hogg, D. W., Lang, D., & Goodman, J. 2013, PASP, 125, 306
Gómez, F. A., Minchev, I., O'Shea, B. W., et al. 2013, MNRAS, 429, 159
Gómez, F. A., White, S. D. M., Marinacci, F., et al. 2016, MNRAS, 456, 2779
Green, G. M., Schlafly, E. F., Finkbeiner, D. P., et al. 2015, ApJ, 810, 25
Hayden, M. R., Bovy, J., Holtzman, J. A., et al. 2015, ApJ, 808, 132
Kruit, P. 1998, Journal of Vacuum Science Technology B: Microelectronics and Nanometer Structures, 16, 3177
Levine, E. S., Blitz, L., & Heiles, C. 2006, ApJ, 643, 881
Liu, C., Fang, M., Wu, Y., et al. 2015, ApJ, 807, 4
Liu, C., Tian, H.-J., & Wan, J.-C. 2017a, in IAU Symposium, 321, Formation and Evolution of Galaxy Outskirts, eds. A. Gil de Paz, J. H. Knapen, & J. C. Lee, 6 (arXiv: 1702.02233)
Liu, C., Xu, Y., Wan, J.-C., et al. 2017b, arXiv:1701.07831
López-Corredoira, M., Cabrera-Lavers, A., Garzón, F., & Hammersley, P. L. 2002, A&A, 394, 883
López-Corredoira, M., & Molgó, J. 2014, A&A, 567, A106
Martig, M., Minchev, I., Ness, M., Fouesneau, M., & Rix, H.-W. 2016, ApJ, 831, 139
Momany, Y., Zaggia, S., Gilmore, G., et al. 2006, A&A, 451, 515
Newberg, H. J., Yanny, B., Rockosi, C., et al. 2002, ApJ, 569, 245
Pohlen, M., & Trujillo, I. 2006, A&A, 454, 759
Roškar, R., Debattista, V. P., Stinson, G. S., et al. 2008, ApJ, 675, L65
Roškar, R., Debattista, V. P., Brooks, A. M., et al. 2010, MNRAS, 408, 783
Shen, J., & Sellwood, J. A. 2006, MNRAS, 370, 2
Stello, D., Huber, D., Bedding, T. R., et al. 2013, ApJ, 765, L41
Tian, H.-J., Liu, C., Wan, J.-C., et al. 2016, arXiv:1603.06262
Wan, J.-C., Liu, C., Deng, L.-C., et al. 2015, RAA (Research in Astronomy and Astrophysics), 15, 1166 (Paper I)
Wu, Y., Luo, A. L., Li, H. N., et al. 2011, RAA (Research in Astronomy and Astrophysics), 11, 924
Wu, Y., Du, B., Luo, A.-L., et al. 2014, IAUS, 306, 340
Xu, Y., Newberg, H. J., Carlin, J. L., et al. 2015, ApJ, 801, 105
Yao, S., Liu, C., Zhang, H.-T., et al. 2012, RAA (Research in Astronomy and Astrophysics), 12, 772
Zhao, G., Zhao, Y.-H., Chu, Y.-Q., Jing, Y.-P., & Deng, L.-C. 2012, RAA (Research in Astronomy and Astrophysics), 12, 723
Zheng, Z., Thilker, D. A., Heckman, T. M., et al. 2015, ApJ, 800, 120